**Chemistry & Biology, Volume *22***

## Supplemental Information

# Non-canonical Bromodomain within DNA-PKcs Promotes DNA Damage Response and Radioresistance through Recognizing an IR-Induced Acetyl-Lysine on H2AX

**Li Wang, Ling Xie, Srinivas Ramachandran, YuanYu Lee, Zhen Yan, Li Zhou, Krzysztof Krajewski, Feng Liu, Cheng Zhu, David J. Chen, Brian D. Strahl, Jian Jin, Nikolay V. Dokholyan, and Xian Chen**

# A non-canonical bromodomain module within DNA-dependent protein kinase promotes DNA damage response and radioresistance through recognizing a radiation-inducible lysine acetylation on H2AX

Li Wang[1,2], Ling Xie[2], Srinivas Ramachandran[2,3], YuanYu Lee[2], Zhen Yan[2,5], Li Zhou[2], Krzysztof Krajewski[2], Feng Liu[4,7], Cheng Zhu[2], David J. Chen[8], Brian D. Strahl[2], Jian Jin[6], Nikolay V. Dokholyan[2,3,10], & Xian Chen[1,2,3,4,9]

[1]Department of Chemistry & Institutes of Biomedical Sciences, Fudan University, Shanghai 20032; [2]Department of Biochemistry & Biophysics; [3]Program in Molecular & Cellular Biophysics; [4]Lineberger Comprehensive Cancer Center, University of North Carolina at Chapel Hill, Chapel Hill, NC 27599, [5]Zhengzhou University, Zhengzhou 450001, China, [6]Departments of Structural and Chemical Biology, Icahn School of Medicine at Mount Sinai, NY 10029, [7]Department of Medicinal Chemistry, Soochow University, Suzhou 215123, China, and [8]Department of Radiation Oncology, UT Southwestern Medical Center, TX 75390.

[9]the overall correspondence should be addressed to, E-mail: xianc@email.unc.edu (X.C.), and [10]regarding molecular modeling to, E-mail: dokh@email.unc.edu (N.D.)

**Table S1** RMSD Comparison of Structural Alignment of DNA-PK with Other Proteins (Related to Figure 2 and 4).

| **Comparison**[1] | **Number of Residues Considered in Alignment**[2] | **Dali Z-score**[3](Holm and Rosenstrom, 2010) | **Cα RMSD**[4] |
|---|---|---|---|
| DNA-PK with Kinase (1E8X) | 215 | 22.1 | 1.6 Å |
| DNA-PK with Bromodomain (3JVK) | 51 | 5.1 | 2.1 Å |

[1]Different regions of DNA-PK (3KGV) compared to kinase and bromodomain structures. [2]The number of residues that returned a significant homology, and were considered for final structural alignment. [3]Z-score obtained upon structure comparison using Dali server: a Z-score above 2 indicates statistically significant structural homology [4]Root Mean Square Deviation of Cα atoms after structural alignment using Dali server[a].

**Table S2** Docking results of the regions of best alignment between DNA-PKcs sequence and the query structure (as determined by FUGUE) (Related to Figure 2).

| JQ1-Crystal Structure[1] | | | -38.4 | 2 | 0.9 |
|---|---|---|---|---|---|
| **FUGUE Hit** | | | **Near Native Cluster** | | |
| **Query[2]** | **Start[3]** | **End[3]** | **Docking Score** | **Rank** | **RMSD** |
| 1WUG | 2071 | 2182 | -34.4 | 9 | 1.1 |
| 1E6I | 2078 | 2180 | -31.5 | 204 | 2.5 |
| 3JVK | 2089 | 2201 | -34.4 | 3 | 0.9 |
| 2H60 | 2680 | 2784 | -24.6 | 38 | 2.8 |
| 1F68 | 3038 | 3149 | -25.0 | 775 | 1.3 |

[1]The first row of the table indicates the docking results of the JQ1-Brd4 crystal structure
[2]PDB ID of the bromodomain structure that was used as a query in FUGUE
[3]The start and end point in the sequence of DNA-PKcs (Uniprot ID: P78527)

**Table S3.** PCR Primers for cloning and mutagenesis of Tip60, H2AX, DNA-PKcs bromodomain and BRD4 (1) (Related to Figure 1, 3, 5, and 6).

| | | |
|---|---|---|
| Tip60 | sense primer | 5'-ggaattctatggcggaggtggtgagtccggtg-3' |
| | anti-sense primer | 5'-cctcgagtcaccacttccccctcttgctccag-3' |
| H2AX mutant K5A | sense primer | 5'-gtcgggccgcggcgcgactggcggcaaggccc-3' |
| | anti-sense primer | 5'-gggccttgccgccagtcgcgccgcggcccgac-3' |
| Wild type DNA-PKcs BRD | sense primer | 5' -ctaggcggccgcatggagcagcgggaccccac- 3' |
| | anti-sense primer | 5' -ctagtctagatcaggccaagcctgtccatgaaag- 3' |
| DNA-PKcs BRD P2110A | sense primer | 5'-agaagcctgggcgcgcctcaaggag-3' |
| | anti-sense primer | 5'-ctccttgaggcgcgcccaggcttct-3' |
| DNA-PKcs BRD N2175A | sense primer | 5'-gcagctggctgcttctgaagccaatggaggagaaggaatt-3' |
| | anti-sense primer | 5'-aattccttctcctccattggcttcagaagcagccagctgc-3' |
| DNA-PKcs BRD M2185A | sense primer | 5'-tggaggagaaggaattcacgccatggtggttgagatagtg-3' |
| | anti-sense primer | 5'-ggccactatctcaaccaccgcgtagtgaattccttctcct-3' |
| DNA-PKcs BRD BRD4(1) | sense primer | 5'-ctaggatatcatgtctgcggagagcggccct-3' |
| | anti-sense primer | 5'-ctagctcgagtcaggagcagccaacacagcaa-3' |

## Figure Legends

**Figure S1.** Analysis of full-length H2AX by FTICR MS. (**A**) Histone extracts from 293T cells were separated by C8 reversed-phase HPLC as the indicated chromatogram and each fraction was collected and the purity of each histone separation was shown by SDS-PAGE. As indicated by red arrow the fraction 19 contained H2AX and the top-down analysis of the fraction 19 is given with the full-length H2AX indicated by red circles. Note that the major component indicated by the black stars is H2B isoforms. (**B**) ECD MS/MS fragment ion ladders as marked in the H2AX full-length sequence showing K5Ac and phospho-Ser139. (**C**) Sequence assignment for each MS signal based on the ECD MS/MS fragment ion ladders as marked in (**B**). **(D)** ECD MS/MS fragment ion ladders as marked in the H2AX full-length sequence showing K5Ac, γSer139 and γTyr142. **(E)** Sequence assignment for each MS signal was based on **(D).** (Related to Figure 1)

**Figure S2.** The abundance correlations between K5Ac and γSer139 or γTyr142 or both when different types of the cells exposed to IR or the DNA damage-inducing chemical (bleomycin). (**A**) IR-induced simultaneous increases of both lysine 5 acetylation and serine 139 phosphorylation in all 293T, HeLa, and U-2 OS cells in a dose-dependent manner while the level of phosphor-Tyr142 remained little changed. (**B**) The HeLa cells treated with bleomycin at the indicated concentrations (0, 5, 10, 25, and 50μg/ml) were lysed at 1, 2, and 4 hours after radiation for immunoblotting. (Related to Figure 1)

**Figure S3.** Hits from aligning bromodomain helices to DNA-PKcs structure using *Situs*. Locations of the hits on the DNA-PKcs structure are shown, with numbers indicating the hit number (A). The kinase structure is shown in blue, with which hit 6 coincides. Hit 2 (**B**) shows good alignment with PKcs helices and a significant *Dali* score (4.6), but also features clashes with adjacent helices (shown in blue, the clashing regions are shown with arrows), hence hit 2 was not selected. Hits 3 (C), 4 (D), 5(E) and 6(F) feature some of the helices of the bromodomain aligning well with DNA-PKcs helices, while other helices are in different orientations and feature clashes with adjacent regions. Arrows denote the unaligned helices. The

unaligned helices preclude us from calculating a *Dali* score for these models. (Related to Figure 2 and 4).

**Figure S4.** Sequence alignment between DNA-PKcs and sequence corresponding to 3JVK (crystal structure of mouse Brd4) as determined by FUGUE reveals 59% similarity between positions in DNA-PKcs and evolutionarily conserved residues of BRD4. The shaded regions represent conserved residues in BRD4, green colored positions represent identical conserved residues and cyan colored positions represent similar conserved residues. The secondary structure of 3JVK (as determined using DSSP(Kabsch and Sander, 1983)) and the predicted secondary structure of DNA-PKcs (using JPred(Cole et al., 2008)) are also shown, denoted as 3JVK SS and DNA-PKcs SS respectively. The prediction confidence of DNA-PKcs secondary structure is denoted as DNA-PKcs SS Conf. The aligned regions of the secondary structures are shown in red. (Related to Figure 4)

**Figure S5.** Structural overlay of DNA-PKcs-BRD-JQ1 near-native binding pose and JQ1-mouse Brd4 co-crystal structure. The BRD homology model is shown in green, while the mouse BRD4 is shown in blue. The proteins are shown with the cartoon representation, while JQ1 is shown with sticks representation. (Related to Figure 2)

**Figure S6.** Circular dichroism (CD) spectra of the refolded secondary structures of the wild-type (WT) DNA-PK-BRD, the DNA-PK-BRD mutants of PN and PNM. (Related to Figure 3).

**Figure S7.** Competition to or removal of K5ac on H2AX affects the association between H2AX and activated DNA-PKcs**. (A)** JQ1 binding of exogenously expressed DNA-PKcs-BRD. (**B**) Comparative analysis of co-localization between activated DNA-PKcs (red, indicated by pT2609) and either FLAG-tagged wild-type (WT) H2AX or the K5A mutant of H2AX. The merged/co-localized pT2609 DNA-PKcs and γH2AX foci in nuclei are depicted in yellow. Nuclei are DAPI-stained in blue. The scale bar is 10 μm. (**C**) Immunoblot analysis of the levels of K5ac or γ-Ser139 on H2AX in chromatin isolated from the same set of cells as described in (**B**). (Related to Figure 4, 5, and 6).

## Supplemental Experimental Procedures

**μESI-FTICR-MS and ECD MS/MS analysis for sequencing full-length H2AX.** Molecular weight determinations of proteins were performed using the "Charge Deconvolution" utility implemented in the DataAnalysis software. The "Resolved-isotope deconvolution" function was enabled to determine the charge state of precursor ions. The cutoff of abundance and charge envelop was set at 10% and 75%, respectively. No smoothing algorithm was used during all data analysis. All other parameters (*e.g.*, High mass=100,000; Min. peaks in comp=3; MW agreement (0.01%)=Auto) were set to default values unless otherwise specified. FTICR-ECD MS/MS was employed to sequence full-length H2AX and its modified forms. 100 MS/MS scans per spectrum were acquired with a resolution of 580,000 at m/z 400 Da. The resulting MS/MS fragments were searched against the full sequence of histone proteins using BioTools software package (Version 3.1, Bruker Daltonics) with the settings described previously(Zhao et al., 2010).

**Cell treatments with DSB-inducing chemicals.** Bleomycin was also used as a DNA damage-inducing reagent and cells were treated at the dose and recovery time as indicated.

**Plasmids and transfection.** The construct of cDNA encoding human histone acetyl transferase Tip60 (GenBankTM accession number 36287048) was generated by PCR with a set of primers: 5'-GGAATTCTATGGCGGAGGTGGTGAGTCCGGTG-3' and 5'-CCTCGAGTCACCACTTCCCCCTCTTGCTCCAG-3'. Tip60 or wild-type H2AX gene was cloned into the expression vector of pcDNA4 vector which was modified by inserting a sequence of FLAG tag located in the N-terminal between the BamHI site and EcoRI site. The point mutation of H2AX K5A was performed using the Quikchange site-directed mutagenesis kit (Stratagene) according to the manufacturer's instructions using wild type FLAG-H2AX as template and using the following primers: 5'-GTCGGGCCGCGGCGCGACTGGCGGCAAGGCCC-3', and 5'-GGGCCTTGCCGCCAGTCGCGCCGCGGCCCGAC-3'. All the constructs were further confirmed by DNA sequencing assay. 1μg of FLAG-Tip60 or FLAG-H2AX (wild type) or FLAG-H2AX K5A (mutant) plasmid was transfected into selected cells by using Superfect transfection reagent. The medium was replaced by a fresh one 4 hours after the transfection and the transfected cells were incubated at 37$^{o}$C for further analysis or other treatments.

**Structural homology between DNA-PKcs and bromodomains (BRDs).** The crystal structure of DNA-PKcs(Sibanda et al., 2010) features various regions named head, forehead, putative DNA-binding domain, and ring structure(Sibanda et al., 2010) (Protein Data Bank (PDB)(Berman et al., 2000) ID: 3KGV). We used bromodomain 1 of mouse Brd4 (PDB ID: 3JVK) and bromodomain from histone acetyltransferase PCAF (PDB ID: 2RNX) as representative templates to search for the presence of bromodomains in DNA-PKcs DNA-PKcs using Situs(Wriggers, 2009). Only the helices from the bromodomain structures were used for the alignments, since the DNA-PKcs structure is of low-resolution and does not feature loops. Furthermore, all residues were modified to alanine, as the side-chain atoms were also not present in the DNA-PKcs structure. Situs was used to facilitate alignment between simulated electron

densities of the low-resolution DNA-PKcs structure, rather than using direct structural alignment using atomic positions, since the connectivity between different secondary structure segments in the DNA-PKcs structure is also unknown. Upon visual inspection, alignment of 3JVK with DNA-PKcs yielded the best fit. Out of the six best hits of 3JVK with DNA-PKcs obtained using Situs, only the best hit was unique and plausible. The other hits could be ruled out based on a variety of reasons (Suppl. Fig. 3). The region of DNA-PKcs that aligned well with 3JVK was culled and used to quantitatively estimate the structural homology with 3JVK using the Dali server(Holm and Rosenstrom, 2010), which is a tool for 3D alignment of protein structures and reports the statistical significance of such alignments. To ensure that the structural alignment we observed was not due to the fact that BRDs resemble two HEAT repeats, we performed a reverse search by taking only the helical regions of BRD and scanning the PDB for similar structures using *Dali*. Even though there are many protein structures in the PDB that contain HEAT repeats, none of these structures, when structurally aligned with BRD, resulted in a Z-score above 5. The absence of other HEAT repeat-containing proteins with Z-scores above 5 suggests that the structural match between BRD and DNA-PKcs is not due simply to the bromodomain resembling two HEAT repeats.

**Constrained DMD simulations of H2AX and DNA-PK.** The DMD simulation methodology is previously described in detail(Ding et al., 2008; Dokholyan et al., 1998). We use CHARMM19 non-bonded potentials(Brooks et al., 1983), EEF1 implicit solvation parameters(Lazaridis and Karplus, 1999) and geometry-based hydrogen bond potentials in DMD(Ding et al., 2008) to model various macromolecular interactions. The time unit of the all-atom DMD simulations is ~50 femtosecond (Brooks et al.) and the temperature is maintained using Anderson's thermostat(Anderson, 1980). We placed H2AX near DNA-PKcs and performed DMD simulations. The DNA-PKcs structure was held static since the structure is incomplete and the residue identities are not known. The simulations were performed with the following constraints: 1) Between H2AX Ser139 and the region adjacent to the catalytic loop of the kinase domain. The region adjacent to the catalytic loop was determined from PI3K structure that was aligned to the DNA-PKcs structure (Fig. 2a-c). 2) Between H2AX Kac and its corresponding binding site at the putative bromodomain. The N6-acetyl-lysine binding site on the putative binding site was determined using the corresponding binding site of the bromodomain template that was aligned to the DNA-PKcs structure (Fig. 2a-c).

**Construction of homology models.** Using the alignments obtained from FUGUE(Shi et al., 2001), the sequence of the template structures were changed to that of aligned regions of DNA-PKcs (listed in Table below) using Medusa(Ding and Dokholyan, 2006; Yin et al., 2007a, b). Insertions and deletions were processed using DMD simulations(Ding et al., 2008; Dokholyan et al., 1998), where most residues of the homology models were maintained static, while residues flanking the insertions and deletions and the residues corresponding to insertions were minimized. Lowest energy structures obtained from $10^6$ steps of constrained simulation was then processed using Chiron (Ramachandran et al., 2011) in the presence of the inhibitor JQ1(Filippakopoulos et al., 2010), to minimize steric clashes. The minimized structure was then used for further docking studies.

**Docking studies.** JQ1 was docked to minimized homology models using MedusaDock (Ding et al., 2010). MedusaDock uses both a flexible receptor and a flexible ligand to arrive at

energetically favorable docking poses of the ligand with the receptor. We performed 25 runs of MedusaDock, each starting with a different random seed to generate a total of ~1000 docking poses for each homology model and also for the crystal structure of Brd4 bound to JQ1 (PDB ID: 3MXF). The docking poses were then clustered based on the root mean square deviation (RMSD) of the drug between two poses. For clustering, we used k-means algorithm with a cut-off of 1-2 Å RMSD in the OC suite(Barton, 1993, 2002 ). We ranked clusters based on cluster size (number of poses in a given cluster). A pose in the top few clusters indicates that it is well sampled. The docking score is described in detail(Ding et al., 2010).

**Expression Plasmid, Expression, Purification, and Refolding of the DNA-PKcs BRD fragments.** The bacterial expression construct p-Gex6p-1878-2700 that expresses DNA-PK was made in the lab of David J. Chen. The PCR fragment of DNA-PKcs (residue 1878-2700) was sub-cloned into BamHI/XhoI sites of p-Gex6p-1, and then a His tag was added to the C-terminal of the gene to generate a dual-tagged GST-His-DNA-PKcs(1878-2700) construct. Sit-directed mutagenesis of DNA-PKcs (N2176A, P2110A/N2176A) was preformed with the QuickChange reagent (Stratagene). Colonies of *E. coli* BL21 cells transformed with pGex6p-1-DNA-PKcs were grown in 2 × YT microbial medium (Sigma) with 100 μg/ml ampicillin, 25 μg/ml chloramphenicol at $37^0$C. Following an induction with 0.1 mM IPTG the cells were allowed to grow overnight at $25^0$C. The cells were collected by centrifugation at 4500rpm for 30 min and the pellet was buffered in 50 mM Tris-HCl (PH 8.0), 5 mM EDTA and 1 mM PMSF, and lysed by passing through Nano DeBee homogenizer at 18,000psi. The inclusion bodies were harvested by centrifugation at 8000g for 30 min, firstly washed with 50 mM Tris-HCl (PH 8.0), 5 mM EDTA(wash 1), four times with 1% deoxycholate (DOC)(wash 2-5), and finally with 50 mM Tris-HCl (PH 8.0) to remove detergent. A centrifugation at 8000g for 30 min was used to collect highly purified inclusion bodies. The inclusion bodies were solubilized in 8M Guanidine HCl, 100 mM Tris-HCl (PH8.0) at room temperature overnight. After centrifugation at 15,000rpm for 30 min insoluble particles were removed and the supernatant was incubated with Ni-NTA beads packed in a glass econo-column (Bio-Rad). Following the washes with 8M Urea, 20 mM Tris-HCl (PH 8.0), and 15 mM Imidazole, the denaturing His-tagged protein was eluted by 8M Urea, 20 mM Tris-HCl (PH8.0), and 200 mM Imidazole. The purified, denaturing GST-DNA-PK-His protein was then dialyzed in a PBS buffer containing 1 mM DTT, 5 Mm EDTA, 10%Glycerol, with a sequential decrease of Urea concentration from 8 to 4 to 2 to 1M to 0 at $4^0$C for 12 hours to refold the protein. The correctly folded protein in the supernatant was collected after removing precipitates. The protein concentration was measured using BCA (Pierce). The protein could be further purified by Glutathione agarose (GE health) according to the manufacture's instruction.

**Circular Dichroism (CD) measurements of the secondary structures of refolded DNA-PKs-BRD fragments.** CD spectra were measured on a Chirascan Plus CD Spectrometer | (Applied Photophysics, Inc) at room temperature, using 1mm quartz cuvettes for the far-UV region (190 nm to 250 nm). Band width and scan speed were set as 0.5 nm and 100 nm/min. Protein samples were dissolved to a final concentration of 0.2 mg/mL in 50mM PBS and 10% glycerol.

**Immunoprecipitation, isolation of chromatin fractionation, and immunoblotting analysis.** Briefly cells were lysed in RIPA buffer (50 mM Tris/HCl, pH 7.6, 150mM NaCl, 0.1% SDS, 0.5% NaDeoxycholate, 1% Triton X-100, and 1×cocktail of protease inhibitors). After incubation on ice for 20 min, samples were centrifuged at 13,000 rpm for 10 min at 4 ℃ to recover the

supernatant for further processing. For immunoprecipitation, whole cell lysates were mixed with the indicated antibodies and protein A agarose (Genscript), incubated at 4 $^{o}$C overnight, collected by centrifugation, and washed five times with lysis buffer. The corresponding immunoprecipitated complexes were eluted with 2X SDS gel sample buffer at 95 $^{o}$C and separated on Tris-Glycine SDS-PAGE or NuPAGE 4-12% SDS gels (Invitrogen). Chromatin fractionation was performed according to a previously described method(Hurd et al., 2009) with minor modifications. For immunoblotting, proteins on gels were transferred to PVDF membranes. After blocking, membranes were blotted with indicated antibodies and visualized using an ECL substrate (Denville Scientific, Inc.) detection system (GE).

**Kinase-Glo Assay for measurement of DNA-PKcs activity**. Briefly, the nuclear extracts of K562 cells were prepared as previously described(Yu et al., 2012). Protein concentration was determined by BCA method. Similar to what previously described(Deriano et al., 2005), cell extracts were mixed with pre-swollen DNA cellulose to pull-down DNA-PKcs. The pull-down samples were washed by a buffer (25mM HEPES (PH7.9), 50mM KCl, 10mM MgCl2, 1mM DTT, 1%IGEPAL CA630, and 20% glycerol) twice, and then mixed with 50 µM DNA-PKcs substrate peptide and the activation buffer (42 µg/ml calf thymus DNA, 50mM HEPES (PH7.9), 100mM KCl, 0.2mM EGTA, 0.5mM EDTA, 1mM DTT and 10mM MgCl2, at a total volume of 20 µl. Using a sample without DNA-PKcs as a control, after pre-incubation at 30$^{o}$C for 5 min, 5 µl ATP (50 µM stock) was added to initiate the kinase reaction. The mixture was allowed to continuely react for 90min at 30$^{o}$C. After sitting for 10 min at RT, the DNA cellulose was spin down by centrifugation and the supernatant was transferred into a white 96 well plate, then 25 µl Kinase-Glo plus reagent was added to initiate luciferase reaction at RT for 10 min, and the luminescence signal was measured by SpectraMax M5 Multimode Reader.

**Constructs, transfection and immunoprecipitation**

Construct of Flag-tagged DNA-PKcs (2070-2200) and BRD4 bromodomain 1 (BRD4 (1)) were cloned into pcDNA4/myc-HisA (Invitrogen) by PCR. Each of the single or triple mutant in DNA-PKcs (2070-2200) including P2110A, N2174A, Y2184A, M2185A or P2110A/N2174A/Y2184A (PNM) were introduced using quickchange (Agilent) and PCR primers (table1). U2OS cells were seeded in the plate and transiently transfected empty vector, Flag-DNA-PKcs (2070-2200) wild type and mutants' plasmids, and Flag-BRD4 (1) with jetPRIME (Polyplus) according to the manufacturer's instructions. After 24hrs, the U2OS cells were exposed to 10 Gy ionizing radiation with an X-ray irradiator (RadSource RS2000) and collected after 1h recovery. For immunoblotting analysis, the cells were lysed directly on the plate with 2*SDS-PAGE sample buffer, boiled for 5 min and sonicated for 5s to shear DNA. Then 5% of the whole cell lysate were separated on a 12% SDS-PAGE gel and sent for western blotting with indicated antibodies: γH2AX-S139 (Abcam, ab2365), Flag (Sigma, F1804), Histone H3 (Abcam, ab1791 ), p-c-Jun S63 (Cell signaling, 2361S), PARP (Cell signaling, 9452), γ-tubulin (Abcam, ab11316), Actin (Santa Cruz, sc1615), Ku70 (Santa Cruz, sc56129), DNA-PKcs (Thermo Scientific, MS-423-P1). For H2AX (Abcam, ab11175) immunoprecipitation analysis, the nuclear protein purification and H2AX immunoprecipitation was performed as described previously (Du et al., 2006).

**Immunofluorescence Assay.** Cells were grown on coverslips, differentially irradiated, washed with PBS, fixed with 4% formaldehyde, and permeabilized with 0.1% NP-40 for 5 min at room

temperature. The cells were then incubated in blocking buffer (PBS containing 3% BSA) for 30 min, followed by incubation with the primary antibody, *i.e.*, anti-γH2AX antibody, anti-Tip60, or anti-phospho-T2609 DNA-PKcs antibody. The mixtures were blocked with 1% BSA in PBS for 1 h. Following PBS washing, the cells were incubated with secondary antibody (Alexa-488-conjugated anti-mouse IgG or Alexa-568-conjugated anti-rabbit IgG [Molecular Probes) for 1 h. Following a wash with PBS containing 4,6-diamidino-2-phenylindole (DAPI; Invitrogen), coverslips were mounted onto glass slides using Permount solution (Fisher Scientific). Experiments with a confocal laser scanning microscopy were performed on a LeicaSP2 AOBS upright laser scanning confocal microscope using the 354-nm line of a UV laser and the 488- and 568-nm lines of argon and helium-neon lasers. The images were processed using LCS Lite software (Leica).

**Clonogenic survival assay.**
Trypsinized U2OS cells were plated in triplicated 6 well plate dishes, and treated with DMSO or JQ1 (250nM). Cells were allowed to attach for 12 h, then low dose irradiation (0.1Gy) and high dose irradiation (2Gy) were performed using an RS2000 X-ray irradiator (RadSource). The cells were incubated at $37^0$C for 7-10 days until colonies were visible, then fixing, staining and counting were done as described previously(Gaddameedhi et al., 2012), percent survival at each condition was determined relative to the number of colonies on control plates.

**Immunoprecipitation, isolation of chromatin fractionation, and immunoblotting analysis.**
Cell extracts or immunoprecipitates were obtained, separated, and transferred as previously described with minor modifications(Leng et al., 2010).

## References


**Anderson, H.C. (1980). Molecular dynamics simulations at constant pressure and/or temperature. Journal of Chemical Physics *72*, 10.**

**Barton, G.J. (1993, 2002 ). OC - A cluster analysis program (University of Dundee, Scotland, UK).**

**Berman, H.M., Westbrook, J., Feng, Z., Gilliland, G., Bhat, T.N., Weissig, H., Shindyalov, I.N., and Bourne, P.E. (2000). The Protein Data Bank. Nucleic Acids Res *28*, 235-242.**

**Brooks, B.R., Bruccoleri, R.E., Olafson, B.D., States, D.J., Swaminathan, S., and Karplus, M. (1983). CHARMM: A program for macromolecular energy, minimization, and dynamics calculations. J Comput Chem *4*, 187-217.**

**Cole, C., Barber, J.D., and Barton, G.J. (2008). The Jpred 3 secondary structure prediction server. Nucleic acids research *36*, W197-201.**

**Deriano, L., Guipaud, O., Merle-Beral, H., Binet, J.L., Ricoul, M., Potocki-Veronese, G., Favaudon, V., Maciorowski, Z., Muller, C., Salles, B., *et al.* (2005). Human chronic lymphocytic leukemia B cells can escape DNA damage-induced apoptosis through the nonhomologous end-joining DNA repair pathway. Blood *105*, 4776-4783.**

**Ding, F., and Dokholyan, N.V. (2006). Emergence of protein fold families through rational design. PLoS Comput Biol *2*, e85.**

**Ding, F., Tsao, D., Nie, H., and Dokholyan, N.V. (2008). Ab initio folding of proteins with all-atom discrete molecular dynamics. Structure *16*, 1010-1018.**

**Ding, F., Yin, S., and Dokholyan, N.V. (2010). Rapid flexible docking using a stochastic rotamer library of ligands. J Chem Inf Model *50*, 1623-1632.**

**Dokholyan, N.V., Buldyrev, S.V., Stanley, H.E., and Shakhnovich, E.I. (1998). Discrete molecular dynamics studies of the folding of a protein-like model. Fold Des *3*, 577-587.**

**Du, Y.-C., Gu, S., Zhou, J., Wang, T., Cai, H., MacInnes, M.A., Bradbury, E.M., and Chen, X. (2006). The dynamic alterations of H2AX complex during DNA repair detected by a proteomic approach reveal the critical roles of Ca2+/calmodulin in the ionizing radiation-induced cell cycle arrest. Molecular & Cellular Proteomics *5*, 1033-1044.**

**Filippakopoulos, P., Qi, J., Picaud, S., Shen, Y., Smith, W.B., Fedorov, O., Morse, E.M., Keates, T., Hickman, T.T., Felletar, I., *et al.* (2010). Selective inhibition of BET bromodomains. Nature *468*, 1067-1073.**

**Gaddameedhi, S., Reardon, J.T., Ye, R., Ozturk, N., and Sancar, A. (2012). Effect of circadian clock mutations on DNA damage response in mammalian cells. Cell Cycle *11*, 3481-3491.**

**Holm, L., and Rosenstrom, P. (2010). Dali server: conservation mapping in 3D. Nucleic Acids Res *38 Suppl*, W545-549.**

**Hurd, P.J., Bannister, A.J., Halls, K., Dawson, M.A., Vermeulen, M., Olsen, J.V., Ismail, H., Somers, J., Mann, M., Owen-Hughes, T., *et al.* (2009). Phosphorylation of histone H3 Thr-45 is linked to apoptosis. J Biol Chem *284*, 16575-16583.**

**Kabsch, W., and Sander, C. (1983). Dictionary of protein secondary structure: pattern recognition of hydrogen-bonded and geometrical features. Biopolymers *22*, 2577-2637.**

**Lazaridis, T., and Karplus, M. (1999). Effective energy function for proteins in solution. Proteins *35*, 133-152.**

**Leng, T., Liu, N., Dai, Y., Yu, Y., Zhang, C., Du, R., and Chen, X. (2010). Dissection of DEN-Induced Platelet Proteome Changes Reveals the Progressively Dys-Regulated Pathways Indicative of Hepatocarcinogenesis. Journal of Proteome Research *9*, 6207-6219.**
**Ramachandran, S., Kota, P., Ding, F., and Dokholyan, N.V. (2011). Automated minimization of steric clashes in protein structures. Proteins *79*, 261-270.**
**Shi, J., Blundell, T.L., and Mizuguchi, K. (2001). FUGUE: sequence-structure homology recognition using environment-specific substitution tables and structure-dependent gap penalties. J Mol Biol *310*, 243-257.**
**Sibanda, B.L., Chirgadze, D.Y., and Blundell, T.L. (2010). Crystal structure of DNA-PKcs reveals a large open-ring cradle comprised of HEAT repeats. Nature *463*, 118-121.**
**Wriggers, W. (2009). Using Situs for the integration of multi-resolution structures. Biophys Rev *2*, 21-27.**
**Yin, S., Ding, F., and Dokholyan, N.V. (2007a). Eris: an automated estimator of protein stability. Nat Methods *4*, 466-467.**
**Yin, S., Ding, F., and Dokholyan, N.V. (2007b). Modeling backbone flexibility improves protein stability estimation. Structure *15*, 1567-1576.**
**Yu, Y., Xie, L., Gunawardena, H.P., Khatun, J., Maier, C., Spitzer, W., Leerkes, M., Giddings, M.C., and Chen, X. (2012). GOFAST: an integrated approach for efficient and comprehensive membrane proteome analysis. Analytical chemistry *84*, 9008-9014.**
**Zhao, S., Xu, W., Jiang, W., Yu, W., Lin, Y., Zhang, T., Yao, J., Zhou, L., Zeng, Y., Li, H., *et al.* (2010). Regulation of cellular metabolism by protein lysine acetylation. Science (New York, NY *327*, 1000-1004.**

# Figure S1

A

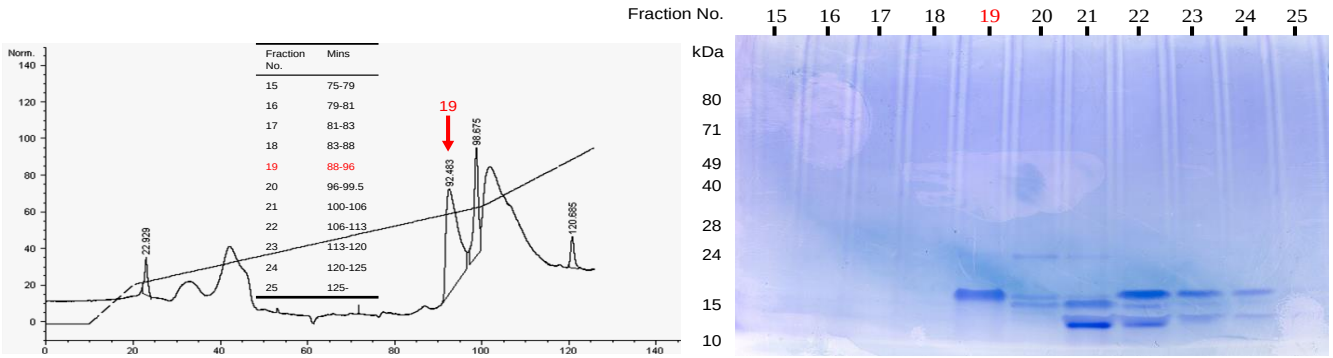


B

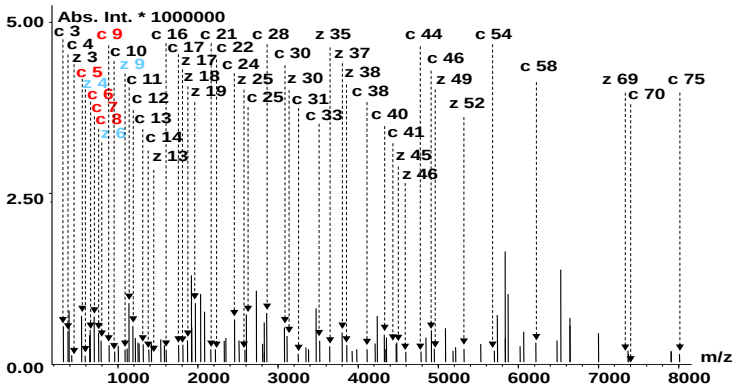


C

SGRGac-KTGGKARAKAKSRSSR
AGLQFPVGRVHRLLRKGHYA
ERVGAGAPVYLAAVLEYLTA
EILELAGNAARDNKKTRIIP
RHLQLAIRNDEELNKLLGGV
TIAQGGVLPNIQAVLLPKKT
SATVGPKAPSGGKKATQAp-SQ
EY

D

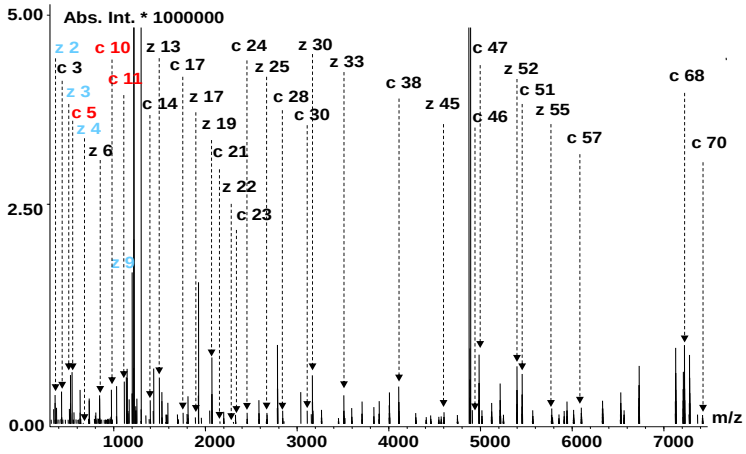


E

SGRGac-KTGGKARAKAKSRSSR
AGLQFPVGRVHRLLRKGHYA
ERVGAGAPVYLAAVLEYLTA
EILELAGNAARDNKKTRIIP
RHLQLAIRNDEELNKLLGGV
TIAQGGVLPNIQAVLLPKKT
SATVGPKAPSGGKKATQAp-SQ
Ep-Y

# Figure S2

A

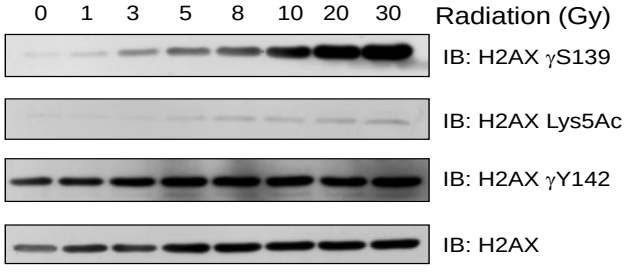
0 1 3 5 8 10 20 30
Radiation (Gy)
IB: H2AX γS139
IB: H2AX Lys5Ac
IB: H2AX γY142
IB: H2AX
293T cells

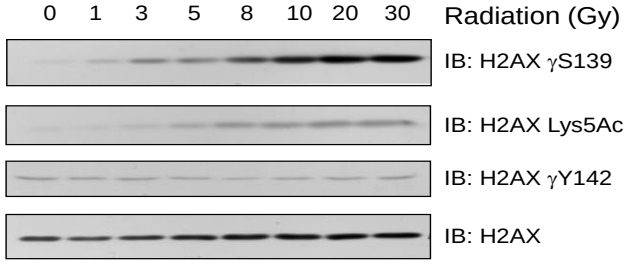
0 1 3 5 8 10 20 30
Radiation (Gy)
IB: H2AX γS139
IB: H2AX Lys5Ac
IB: H2AX γY142
IB: H2AX
HeLa cells

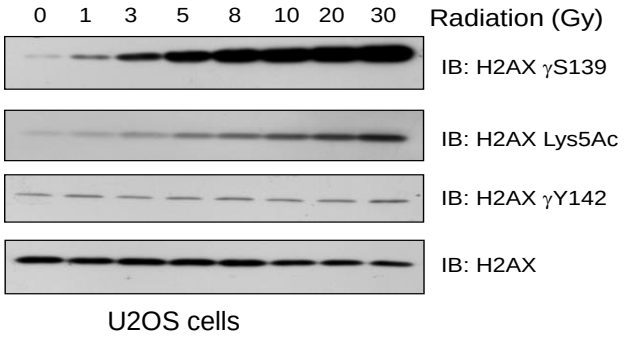
0 1 3 5 8 10 20 30
Radiation (Gy)
IB: H2AX γS139
IB: H2AX Lys5Ac
IB: H2AX γY142
IB: H2AX
U2OS cells

B

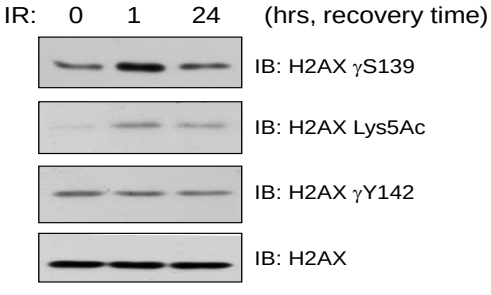
IR: 0 1 24 (hrs, recovery time)
IB: H2AX γS139
IB: H2AX Lys5Ac
IB: H2AX γY142
IB: H2AX
293T cells

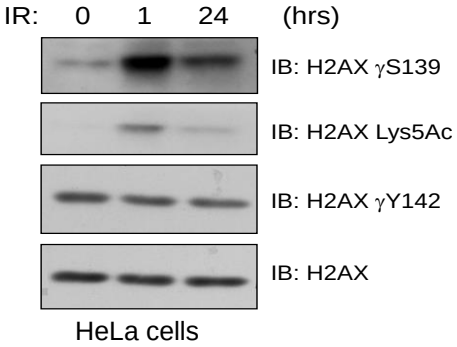
IR: 0 1 24 (hrs)
IB: H2AX γS139
IB: H2AX Lys5Ac
IB: H2AX γY142
IB: H2AX
HeLa cells

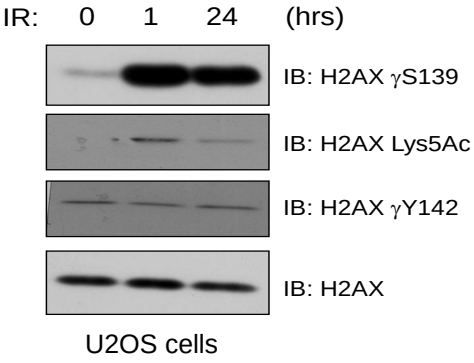
IR: 0 1 24 (hrs)
IB: H2AX γS139
IB: H2AX Lys5Ac
IB: H2AX γY142
IB: H2AX
U2OS cells

Figure S3

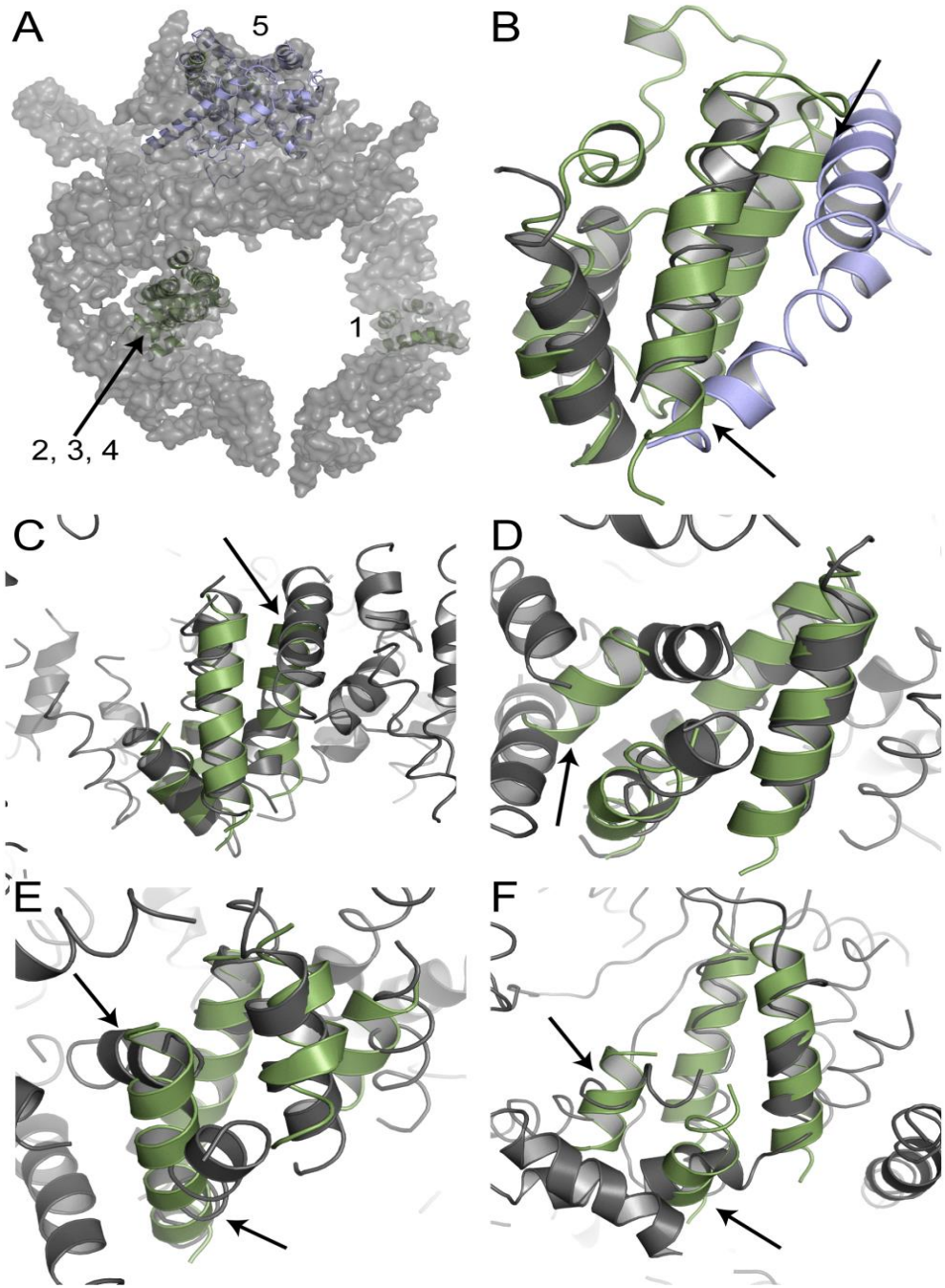

Figure S4

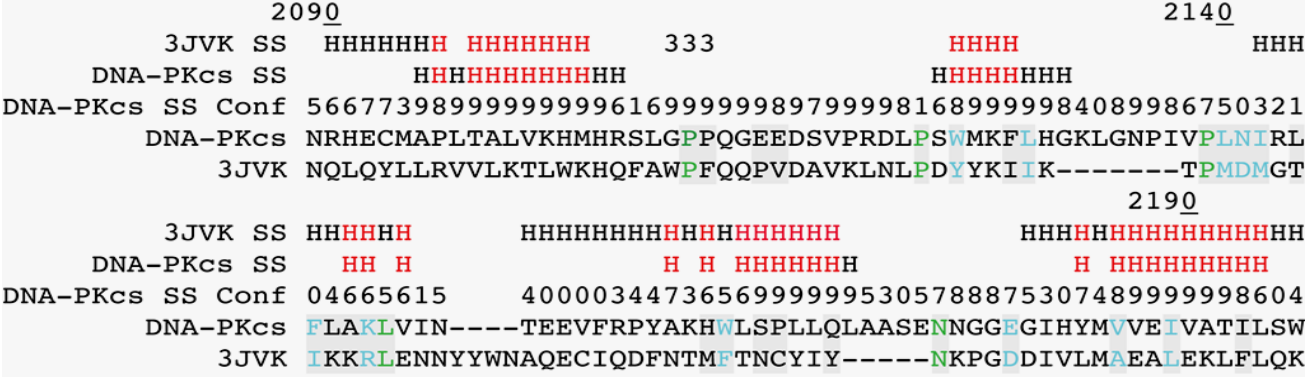
2090
2140
3JVK SS HHHHHHH HHHHHHH 333 HHHH HHH
DNA-PKcs SS HHHHHHHHHHH HHHHHHHH
DNA-PKcs SS Conf 566773989999999961699999989799998168999998408998675032 1
DNA-PKcs NRHECMAPLTALVKHMHRSLGPPQGEEDSVPRDLPSWMKFLHGKLGNPIVPLNIRL
3JVK NQLQYLLRVVLKTLWKHQFAWPFQQPVDAVKLNLPDYYKIIK-------TPMDMGT
2190
3JVK SS HHHHHH HHHHHHHHHHHHHHHHHHH HHHHHHHHHHHHHH
DNA-PKcs SS HH H H H HHHHHHH H H HHHHHHHHH
DNA-PKcs SS Conf 04665615 4000034473656999999530578887530748999999860 4
DNA-PKcs FLAKLVIN----TEEVFRPYAKHWLSPLLQLAASENNGGEGIHYMVVEIVATILSW
3JVK IKKRLENNYYWNAQECIQDFNTMFTNCYIY-----NKPGDDIVLMAEALEKLFLQK

Figure S5

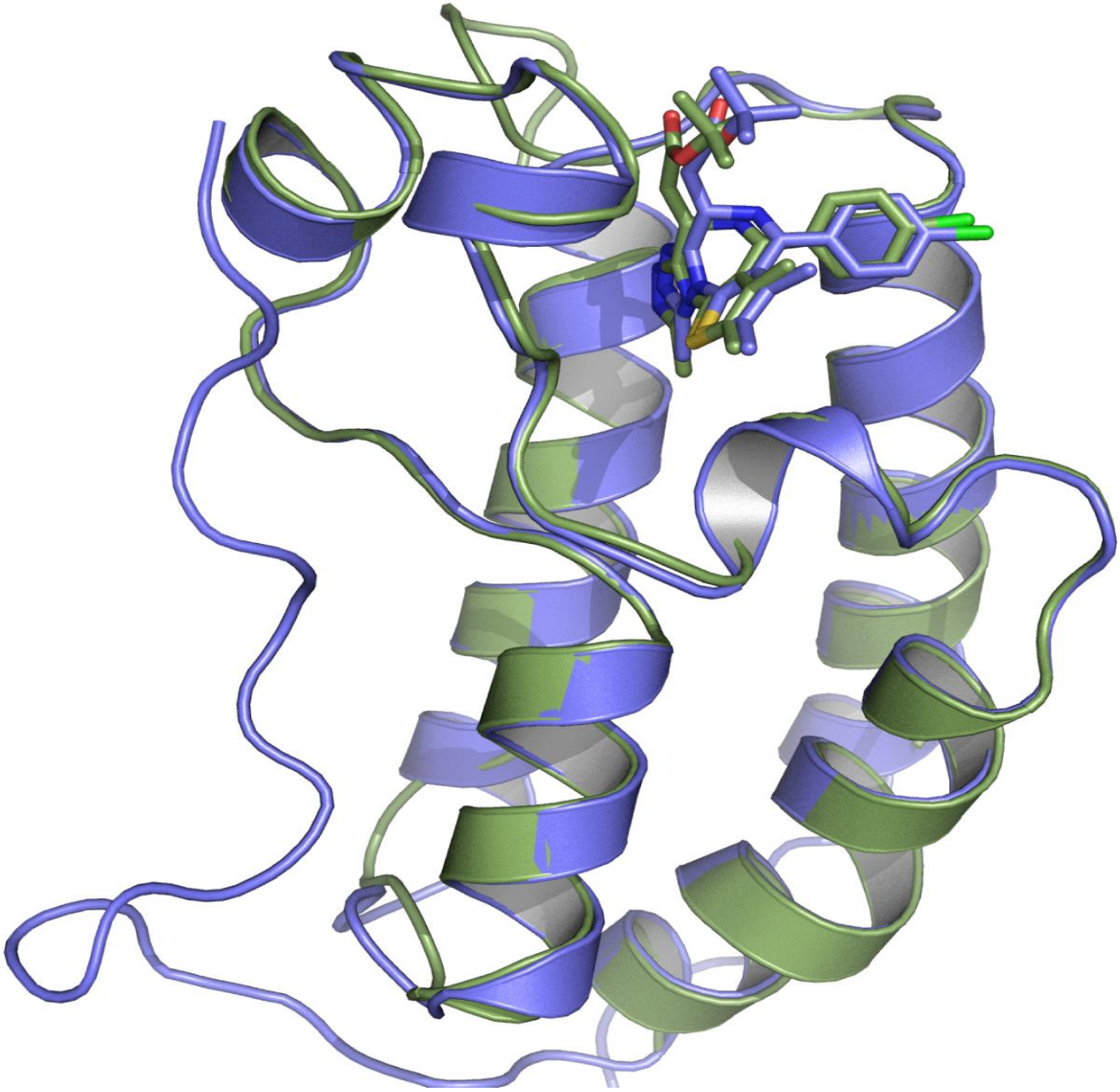

Figure S6

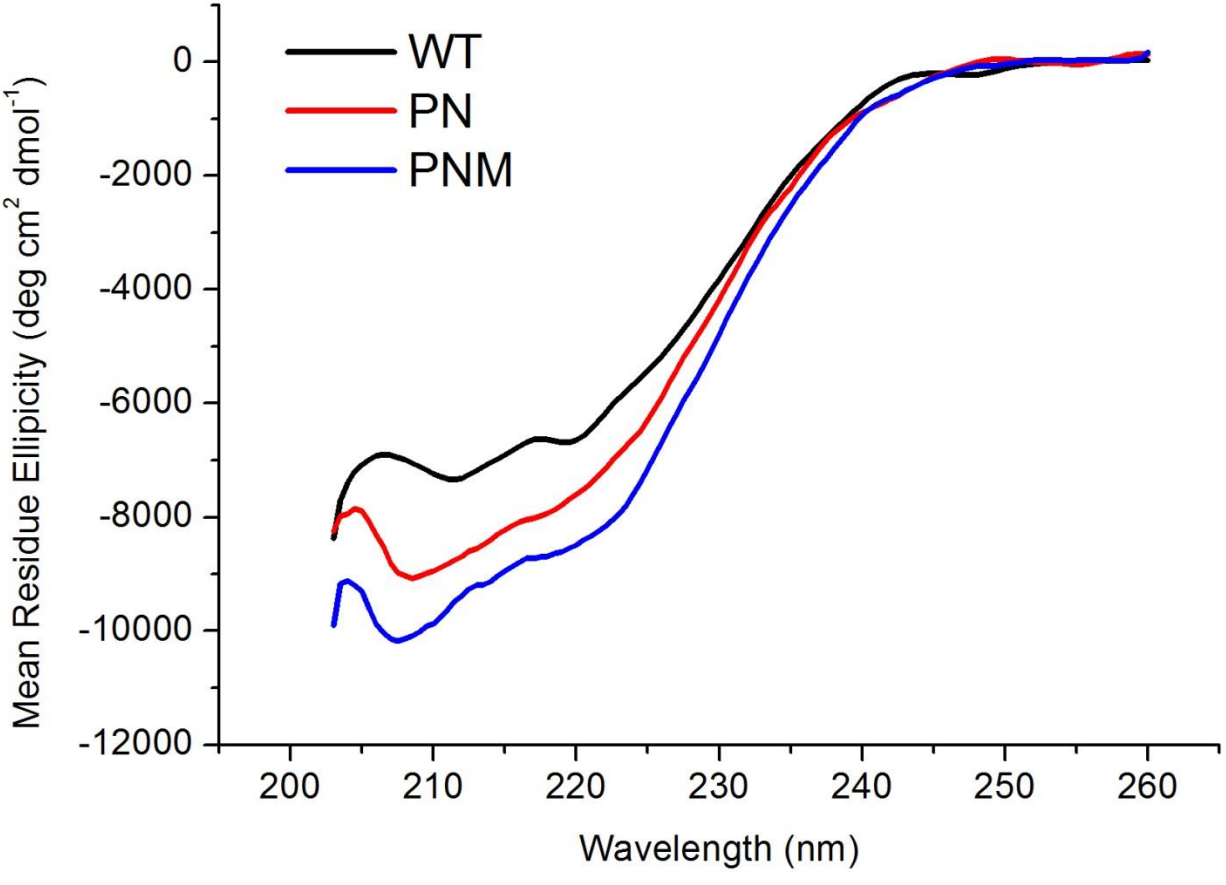
WT
PN
PNM
0
-2000
-4000
-6000
-8000
-10000
-12000
Mean Residue Ellipicity (deg cm2 dmol-1)
200
210
220
230
240
250
260
Wavelength (nm)

Figure S7

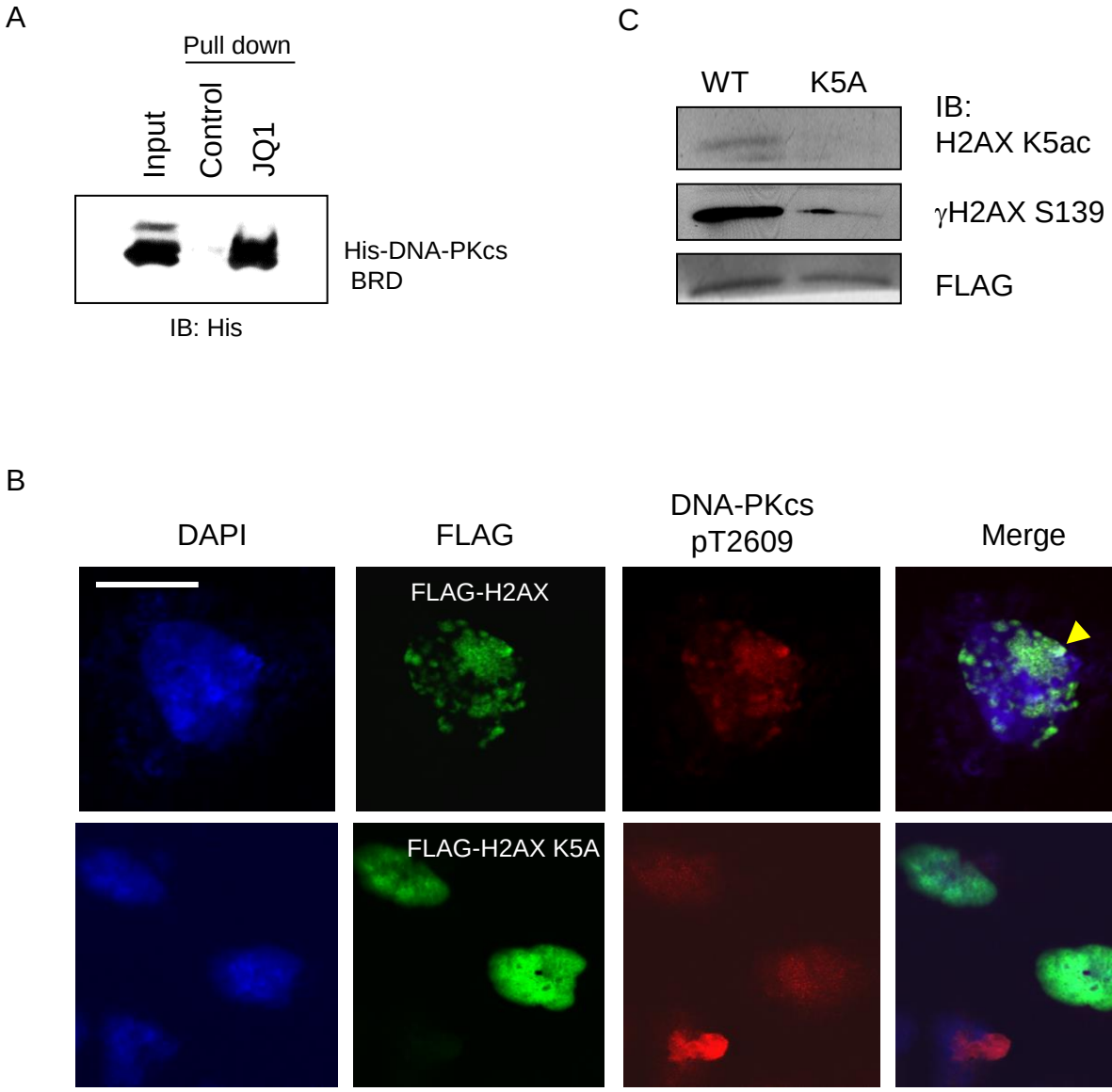
A
Pull down
Input
Control
JQ1
His-DNA-PKcs
BRD
IB: His
C
WT
K5A
IB:
H2AX K5ac
γH2AX S139
FLAG
B
DAPI
FLAG
DNA-PKcs
pT2609
Merge
FLAG-H2AX
FLAG-H2AX K5A